ACS NANO
Cite This: ACS Nano XXXX, XXX, XXX−XXX
www.acsnano.org

ARTICLE

Piezotronic Effect on Rashba Spin−Orbit Coupling in a ZnO/P3HT Nanowire Array Structure

Laipan Zhu,[†,‡,⊥] Yan Zhang,[†,‡,§,⊥] Pei Lin,[†,‡] Ying Wang,[†,‡] Leijing Yang,[†,‡] Libo Chen,[†,‡] Longfei Wang,[†,‡] Baodong Chen,[†,‡] and Zhong Lin Wang*[,†,‡,#]

[†]CAS Center for Excellence in Nanoscience, Beijing Key Laboratory of Micro-nano Energy and Sensor, Beijing Institute of Nanoenergy and Nanosystems, Chinese Academy of Sciences, Beijing 100083, China

[‡]School of Nanoscience and Technology, University of Chinese Academy of Sciences, Beijing 100049, China

[§]School of Physical Electronics, University of Electronic Science and Technology of China, Chengdu 610054, China

[#]School of Material Science and Engineering, Georgia Institute of Technology, Atlanta, Georgia 30332, United States

Supporting Information

ABSTRACT: **A key concept in the emerging field of spintronics is the voltage-gate control of spin precession *via* the effective magnetic field generated by the Rashba spin−orbit coupling (SOC). Traditional external gate voltage usually needs a power supply, which can easily bring about background noise or lead to a short circuit in measurement, especially for nanoscale spintronic devices. Here, we present a study on the circular photogalvanic effect (CPGE) in a ZnO/P3HT nanowire array structure with the device excited under oblique incidence. We demonstrate that a strong Rashba SOC is induced by the structure inversion asymmetry of the ZnO/P3HT hetero-interface. We show that the Rashba SOC can be effectively tuned by inner-crystal piezo-potential created inside the ZnO nanowires instead of an externally applied voltage. The piezo-potential can not only ensure the stability of future spin-devices under a static pressure or strain but also work without the need of extra energy; hence this room-temperature generation and piezotronic effect control of spin photocurrent demonstrate a potential application in large-scale flexible spintronics in piezoelectric nanowire systems.**

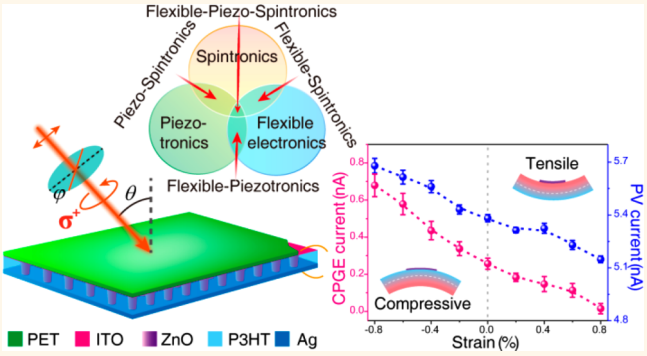

KEYWORDS: *ZnO nanowire array, circular photogalvanic effect (CPGE), Rashba spin−orbit coupling (SOC), piezotronic effect, piezo-potential*

Spintronic devices based on spin-polarized electrons offer the promise of significantly enhanced device performance in terms of speed, size, and power consumption.[1−4] The band spin splitting has been intensively realized *via* the Zeeman effect through the coupling of an external magnetic field and electron spin.[5−7] However, band spin degeneracy can also be removed without the action of an external magnetic field, which is the so-called spin−orbit coupling (SOC) in noncentral symmetric crystals, a relativistic effect allowing for coupling of electron spin and orbital degrees of freedom.[8−10] The SOC, enabling electrical generation, manipulation, and detection of spins in semiconductors, is the key issue in the realization of new spintronic devices. In low-dimensional semiconductors, SOC is believed to originate from the Rashba term induced by structure inversion asymmetry (SIA) and the Dresselhaus term induced by bulk inversion asymmetry (BIA).[8,11,12] The BIA, depending on the lattice size, temperature, and electron density, is due to the absence of a spatial inversion center in the bulk crystal itself, which is usually present in zinc-blende structure materials, while the SIA is usually due to the absence of a spatial inversion center caused by the intrinsic heterostructure asymmetry, which need not be related to the crystal lattice. The SIA may arise from different kinds of asymmetry of the heterostructures such as nonequivalent normal and inverted interfaces, asymmetric doping of quantum wells, asymmetrically shaped quantum wells, and external or built-in electric fields (the larger the built-in electric field is, the stronger the SIA will usually be).[8,13] Therefore, in comparison to the Dresselhaus SOC, the Rashba SOC has attracted much concern, as it can be

Received: December 5, 2017
Accepted: January 22, 2018
Published: January 22, 2018

DOI: 10.1021/acsnano.7b08618
ACS Nano XXXX, XXX, XXX−XXX

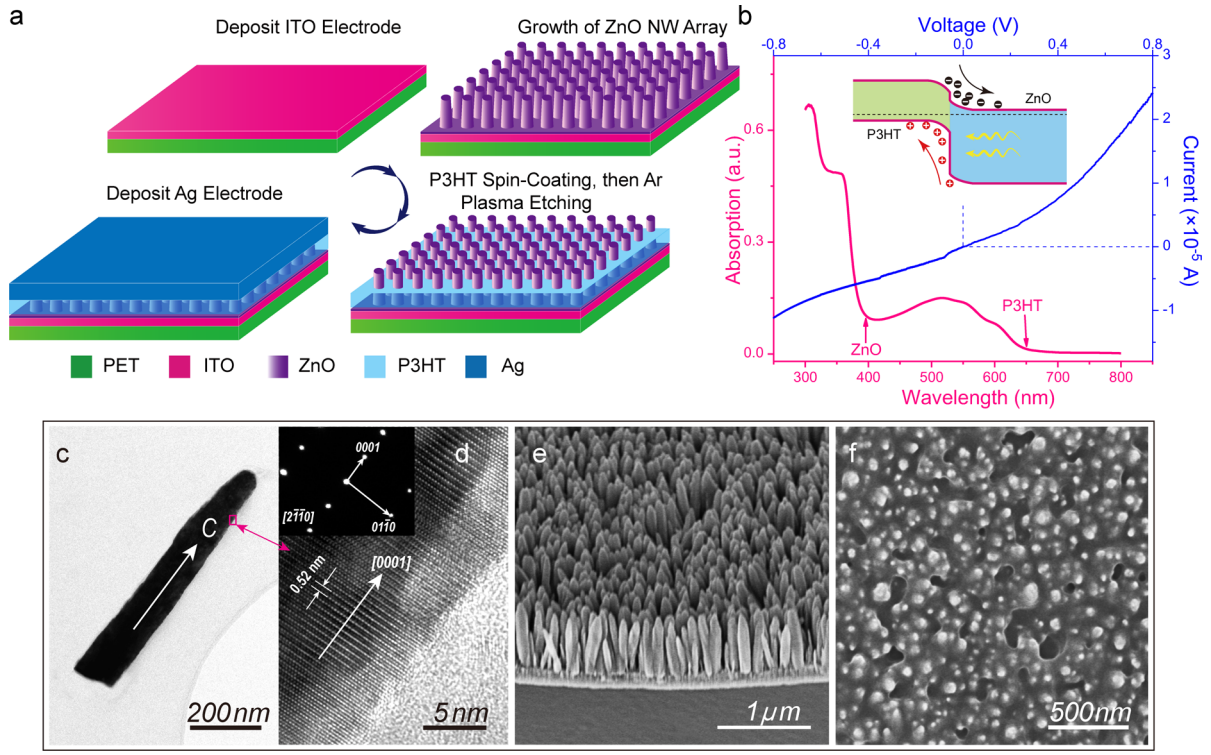

Figure 1. Characterization of the device. (a) Fabrication processes of the device. (b) Spectrum of UV−vis−IR absorption and *I*−*V* characteristics of the device. (c) Low-magnified TEM image of a ZnO NW. (d) HRTEM image of the ZnO NW. The inset in the upper left corner denotes the SAED pattern of the ZnO NW. (e) SEM image showing side view of the as-grown ZnO NW array. (f) SEM image showing top view of the ZnO NW array with spin-coated P3HT.

tailored by artificial microstructure design and modulated by applying a gate voltage.[14−16]

Rashba SOC has been reported in quantum wells, two-dimensional electron gases, and thin films based on III−V compound semiconductors.[15,17−21] Rashba SOC has also been confirmed at the surface of heavy metals such as Au, Ir, or BiAg(111) alloys.[22−24] Recent works reveal that the Rashba effect can also be realized in hybrid organic−inorganic perovskites.[25−27] More recently, topological insulators[28] and transition-metal dichalcogenides[29] have been shown to display strong Rashba SOC. Structures that present bulk inversion asymmetry also show evidence of a Rashba-type spin−orbit splitting of the band structure. For instance, the polar semiconductor BiTeI displays a bulk Rashba SOC as large as that found on the surface of topological insulators.[30] Most recently, giant tunable Rashba spin splitting in a two-dimensional BiSb monolayer was found.[31] It would be desirable if efficient tuning of the Rashba SOC can be achieved in nanowires to accelerate the development of the forthcoming nanospintronic technology. Recently, strong Rashba SOC in semiconductors with one-dimensional nanowire (NW) structure has been observed, such as Ge/Si core−shell single nanowires[14] and InAs single nanowires,[16] which are tuned *via* gate voltages. The external gate voltages were applied *via* a solid electrolyte, a double gate, or a field effect transistor (FET)-like gate.[14,16] However, an external electric field usually needs a power supply, which can easily bring about background noise or lead to a short circuit in measurement, especially for nanospintronic devices. What's more, these devices usually require harsh growth techniques or complex micronanofabrication processes.

Recently, with lower cost, facile-manufactured process, and better piezoelectric performance, much attention has been focused on ZnO NWs for potential applications in ultraviolet optoelectronics, transparent high-power electronics, piezoelectric transducers, *etc.*[32−34] ZnO possesses a wide band gap of 3.4 eV and an exciton binding energy of 60 meV, which will be strongly beneficial to room-temperature operation of future spintronic devices. Attention has also been given to ZnO thin films and quantum dots for the promising property of possible applications in spintronic devices thanks to the long spin relaxation time.[35−39] But the main problem is that these materials usually need to be grown with an intricate and costly process, such as using molecular beam epitaxy technology. However, the ZnO NW can be easily grown with low cost *via* a low-temperature hydrothermal method on arbitrary substrates, still keeping a high-quality crystal orientation. Meanwhile, upon normal stress, owing to the piezotronic effect in the noncentral symmetric ZnO NW wurtzite structure, the piezoelectric polarization charges induced piezo-potential in the NW at the heterojunction or interface can act as a gate voltage to tune and control the current of piezoelectric devices, such as a piezoelectric field effect transistor, strain-gated transistors, and piezotronic logic devices.[34,40−43] It is worth noting that the piezo-potential can not only remain steady under a static pressure or strain, ensuring the stability of future spin-devices, but also work without the need of any extra energy. Therefore, using an inner-crystal piezo-potential instead of an external gate voltage to manipulate the Rashba SOC in NWs will be a great attempt. If the performance of a spin device can be tuned by using a simple external pressure or strain, it would be desirable for future self-powered nanospintronic devices. As far as we know, the manipulation of spin transport by strain itself is low-

DOI: 10.1021/acsnano.7b08618
ACS Nano XXXX, XXX, XXX−XXX

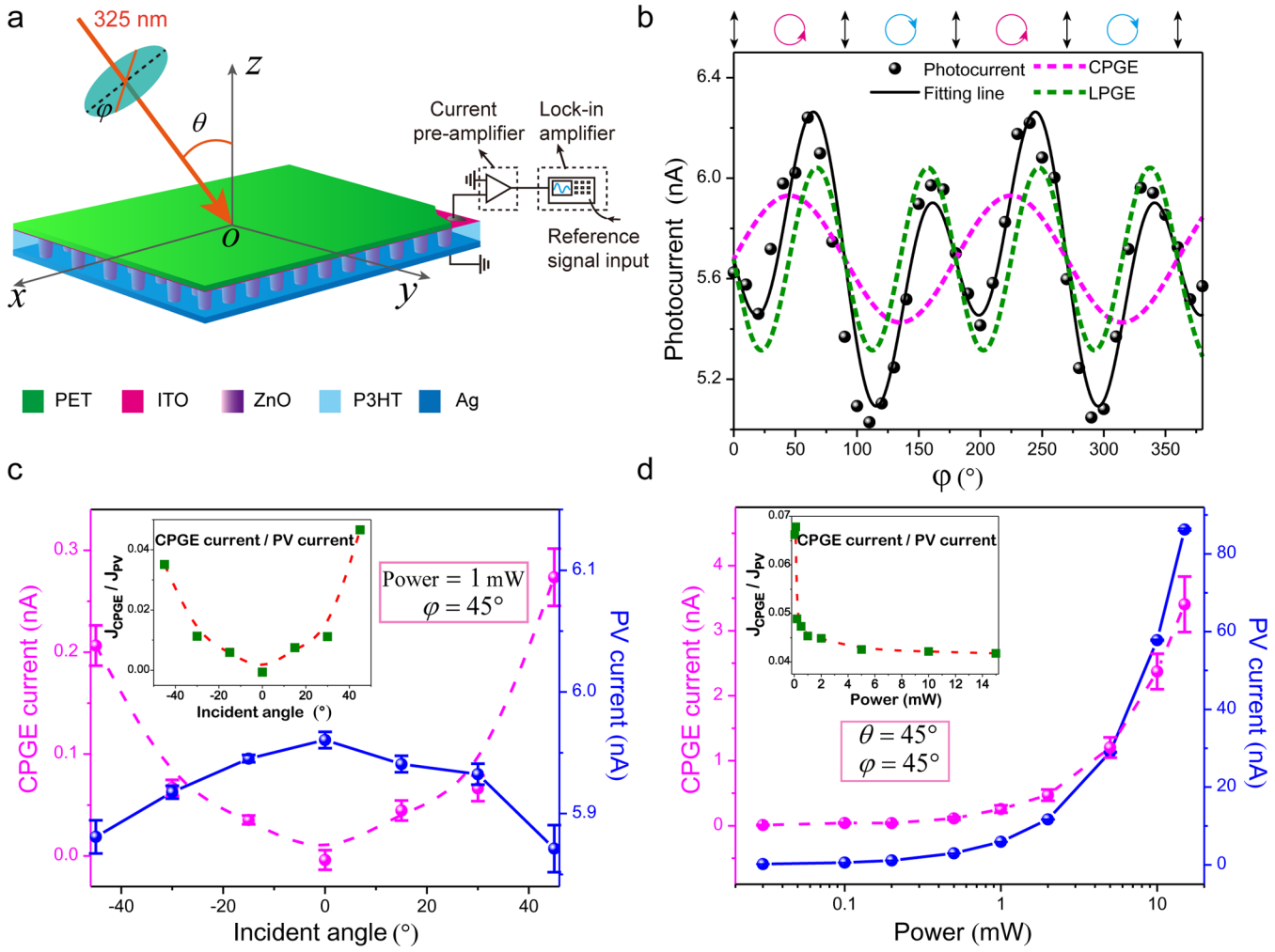

Figure 2. Photocurrent measurement and its dependence on incident angle and light power. (a) Schematic diagram of the setup of CPGE current measurement. (b) Measured photocurrent as a function of the phase angle φ for 45° oblique incidence with 1 mW light irradiation at room temperature. The black line is the fitting line. Both CPGE and LPGE currents are extracted, shown with pink and green dashed lines, respectively. The baseline for the CPGE and LPGE current is actually zero, which is shifted for contrast. (c) Extracted CPGE current and PV current as a function of incident angle. The inset is a normalized CPGE current by the corresponding PV current. (d) Extracted CPGE current and PV current as a function of excitation power of the laser. The inset is a normalized CPGE current by the corresponding PV current.

efficiency. It would be desirable if efficient piezotronic effect tuning of a Rashba SOC can be achieved in NWs to enable future spintronic devices with superior performance.

In this study, a ZnO NW array of ~100 nm in diameter and 800 nm in length is grown on a PET flexible substrate, and a simple ZnO/P3HT interface is fabricated to effectively produce structure inversion asymmetry and thus induce Rashba SOC. Here, P3HT is a p-type polymer, which has a high mechanical property under bending strain. P3HT can also be easily spin-coated around the side surface of the ZnO NWs. We use the circular photogalvanic effect (CPGE), a sensitive method to evaluate the strength of SOC in gyrotropic optical semiconductors with a strong spin−orbit coupling even at room temperature, to study the Rashba SOC in the ZnO/P3HT-based device. Excitingly, using the inner-crystal piezo-potential in the ZnO NW array induced by simply bending the device, the Rashba SOC is found to be effectively manipulated, which is 2.6 times enhanced under a 0.8% compressive strain compared with the unstrained one. The fact that the devices can actually be fabricated directly over a large area of high-density nanowire arrays is quite appealing, as conventional studies are done with a single or few nanowires. This study shows a promising way of spin manipulation *via* the piezotronic effect on large-scale flexible spintronic devices.

RESULTS AND DISCUSSION

The fabrication processes of the device are illustrated in Figure 1a. The UV−vis−IR absorption spectrum denotes exactly the band-edge of optical absorption corresponding to ZnO (~395 nm) and P3HT (~650 nm), respectively (see Figure 1b). The *I*−*V* curve (see Figure 1b) shows an expected poor ohmic contact because of the weak p−n junction (only annealed at 100 °C in air for 2 min) characteristics between n-ZnO and p-P3HT. The device is based on an array of n-ZnO/p-P3HT core−shell nanowires grown on an indium tin oxide (ITO)-coated PET substrate, with the *c*-axis of the ZnO NWs pointing upward from the substrate (see Figure 1c,d). TEM and SEM images (Figure 1c−f and Supporting Information Figure S1) of the as-grown ZnO NW array and ZnO NW array with spin-coated P3HT exhibit a cone-shaped ZnO NW array of about 800 nm in length and 100 nm in bottom diameter. It is worth noting that the surface of the P3HT-coated ZnO NW array was

DOI: 10.1021/acsnano.7b08618
ACS Nano XXXX, XXX, XXX−XXX

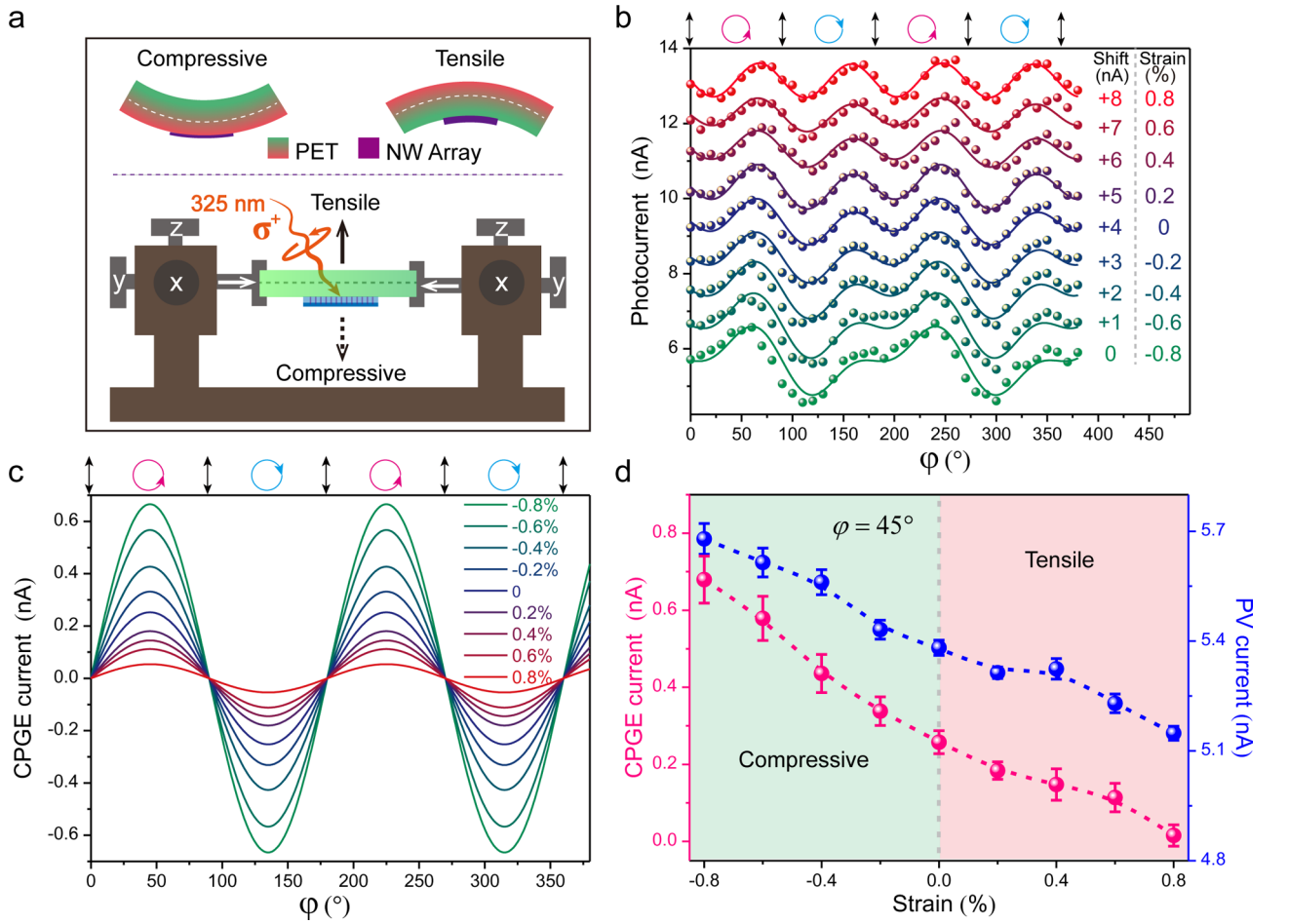

Figure 3. Photocurrents as a function of strain. (a) Setup for the CPGE current measurement under compressive and tensile strains. (b) Measured photocurrents as a function of phase angle φ for oblique incidence of θ = +45° and light intensity of 1 mW under compressive and tensile strains at room temperature. The colored lines are fitting lines. The data and fitting lines are intentionally shifted for clarity. (c) Extracted CPGE currents as a function of phase angle for an oblique incidence of θ = +45° under compressive and tensile strains at room temperature. (d) Amplitudes of CPGE and PV currents as a function of strain for an oblique incidence of θ = +45°.

cleaned by Ar plasma to expose the head of the ZnO NW array for nearly ohmic contact with the Ag electrode (see Figure 1f). The spin-coated P3HT, an organic polymer, can also enhance the tolerance of the device under mechanical forces.

Photocurrent measurement is then illustrated in Figure 2a. We define the $-c$ growth direction of ZnO NWs as the z-axis and the two orthogonal directions perpendicular to the ZnO NW array as the x- and y-axes (see Figure 2a). Semiconductors that support the CPGE are traditionally gyrotropic optical media with a strong spin−orbit coupling, so that the effect is ordinarily controlled by angular momentum selection rules for excitation with left (σ^-)- or right (σ^+)-handed circularly polarized light.[8] The CPGE current can be quantitatively described by

$$j_\lambda = \sum_\mu \chi_{\lambda\mu} \hat{e}_\mu E_0{}^2 P_{\mathrm{circ}} \tag{1}$$

,where j is the photocurrent density, χ is the CPGE second-rank pseudotensor, E_0 is the complex amplitude of the electric field of the electromagnetic wave of the light, P_{circ} is the degree of circular polarization, $\hat{e} = \mathbf{q}/q$ is the unit vector pointing in the direction of light propagation, and $\mathbf{q}$ is the light wave vector inside the medium. χ contains information on the SOC. The helicity of the incident radiation is given by$P_{\mathrm{circ}} = \frac{I_{\sigma^+} - I_{\sigma^-}}{I_{\sigma^+} + I_{\sigma^-}} = \sin(2\varphi)$, where φ is the phase angle between the x- and y-components of the electric field vector. Actually, Zhang *et al.* have reported a strong in-plane CPGE in ZnO epitaxial films (~0.7 μm) under interband excitation, which is believed to be due to the strong SOC in ZnO or the inversed valence band structure of ZnO.[36] However, the ZnO films were grown by a costly technology, called molecular beam epitaxy. In this work, we demonstrate a strong CPGE current in a low-cost n-ZnO/p-P3HT core−shell NW array. The measured photocurrent between the two electrodes of the NW array as a function of the rotation angle φ of the quarter-wave plate is shown in Figure 2b, where the incidence angle is fixed at θ = 45°. The measured photocurrent can be empirically fitted by the expression

$$J_{\mathrm{total}} = J_{\mathrm{CPGE}} \sin(2\varphi) + J_{\mathrm{LPGE}} \sin(2\varphi) \cos(2\varphi) + J_{\mathrm{PV}} \tag{2}$$

,where J_{CPGE} is the amplitude of the CPGE current, J_{LPGE} is the amplitude of the linear photogalvanic effect (LPGE) current which results from asymmetric scattering of electrons or anisotropy of light absorption, and J_{PV} represents the polarization-independent photocurrent originating from the photovoltaic (PV) effect (the small Dember effect induced by the density gradient of photoinduced electrons is ignored in

DOI: 10.1021/acsnano.7b08618
ACS Nano XXXX, XXX, XXX−XXX

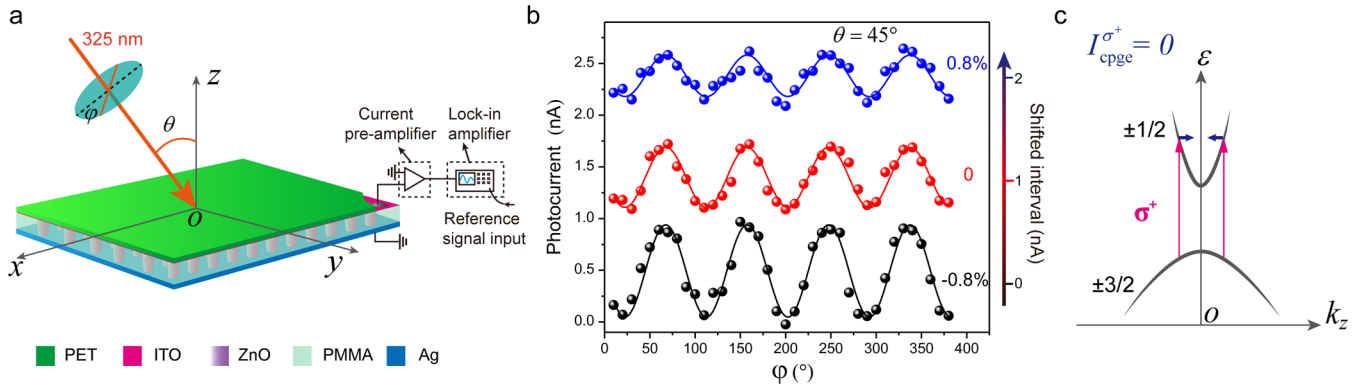

Figure 4. Demonstration of no CPGE current of the ZnO NW array without a P3HT layer. (a) Schematic diagram of the device and setup for CPGE current measurement. (b) Photocurrents as a function of phase angle φ for an oblique incidence of θ = +45° under −0.8% compressive and 0.8% tensile strains at room temperature. The colored lines are fitting lines. The data and fitting lines are intentionally shifted for clarity. (c) Optical transition diagram denoting the zero CPGE current.

this condition).[8] The LPGE current oscillates with angle φ in a period of $\pi/2$, while the CPGE current oscillates with the angle φ in a period of π. As can be seen from the fitting line in Figure 2b, J_{CPGE} and J_{LPGE} are of the same order, while J_{PV} is about one order larger than J_{CPGE} or J_{LPGE}. There is a phase shift between the maximum of the linear polarization of the light and the LPGE signal, which is normal because of the use of the quarter-wave plate (see Figure S2 in the Supporting Information for details). We do not discuss LPGE further more because it has nothing to do with the SOC.

The amplitudes of CPGE and PV currents are extracted respectively as a function of incident angle in Figure 2c (also see Figure S3 in the Supporting Information), in which the inset is the normalized CPGE currents by the corresponding PV currents. The PV currents decrease under both positive and negative incident angles, which is due to the increased reflection and reduced absorption of light at larger incident angles. The n-ZnO/p-P3HT heterointerface with induced built-in electric field causes a structure inversion asymmetry parallel to the direction of the built-in electric field. Thus, a Rashba SOC at the n-ZnO/p-P3HT heterointerface is induced, which further causes a spin splitting of the energy band at the surface (contacting directly with P3HT) of ZnO NWs. Hence a detectable CPGE current is observed under oblique incident light. From the group symmetry point of view, the built-in electric field in the P3HT/ZnO heterojunction lowers the symmetry of the nanowire surface, leading to nonzero items of χ_{zy} and χ_{zx}, which is the origin of the CPGE current in the z-direction (c-axis of ZnO NWs).[8] However, the CPGE currents in Figure 2c increase under both positive and negative incident angles, which is different from the almost linear tendency observed in in-plane samples (parallel to the x−o−y plane) according to previous literature.[36,44−46] In these former studies, the J_{CPGE} can be described by the following phenomenological expression: $J_{CPGE} \propto (\alpha + \beta)I \sin(\theta)$, where α and β are respectively the Rashba and Dresselhaus SOC coefficients, I is the light intensity, and θ is the incidence angle. Apparently, the amplitude of the CPGE current is directly proportional to the total SOC coefficient $(\alpha + \beta)$ and $\sin(\theta)$ with the fixed light intensity. Under small angles ($|\theta| \leq 45°$), one can get $\sin(\theta) \approx \theta$, which is attributed to the almost linear tendency of incidence angle dependence of J_{CPGE} in former studies. However, in this out-of-plane structure, where a spin-related current is detected vertically to the x−o−y plane, a negative incidence of light ($\theta = -\theta_0$, $0° < \theta_0 \leq 45°$) is equivalent to the corresponding positive incidence of light ($\theta = +\theta_0$). Hence, the J_{CPGE} should be described by expression

$$J_{CPGE} \propto (\alpha + \beta)I|\sin(\theta)| \quad (3)$$

We then studied the power dependence of J_{CPGE} (namely, the amplitude of the CPGE current with φ = 45°) and J_{PV} under an incidence angle θ = +45°, as shown in Figure 2d (also see Figure S4 in the Supporting Information). We found that J_{CPGE} and J_{PV} both increase linearly (see Figure S5 in the Supporting Information for the linear x-axis) with light power enhanced from 0.03 to 15 mW. From the inset of Figure 2d, the normalized CPGE current by the corresponding PV current shows a sharp decrease with power enhanced from 0.03 mW to 2 mW but a gentle decrease with power enhanced from 2 mW to 15 mW, which is due to the built-in electric field at the n-ZnO/p-P3HT heterointerface being partially screened by the photovoltaic effect after illumination.[47,48] As a result, the weakened built-in electric field decreases the spin-splitting energy; it is also, in turn, suggested that the spin splitting of the n-ZnO/p-P3HT heterointerface mainly arises from the Rashba effect.[47,48] It should be noted that it is possible to enhance the SOC by improving the crystallinity of ZnO NWs.

The strain dependence of the photocurrents is studied. A schematic diagram for the CPGE current measurement under compressive and tensile strains is shown in Figure 3a. The values of compressive and tensile strains shown in Figure 3 are calculated from the surface deformation of PET with an attached NW array (regardless of the thickness of the NW array), not the values applied directly on the NW array. The measured photocurrents as a function of phase angle φ for oblique incidence of θ = +45° under compressive and tensile strains are shown in Figure 3b, from which we can see that the number of maximum peaks degrades gradually from four to two with increased compressive strain and that the four maximum peaks become comparable gradually with increased tensile strain. By fitting the experimental data using eq 2, we extract the CPGE currents as a function of phase angle for an oblique incidence of θ = +45° under compressive and tensile strains (see Figure 3c). The amplitude of the CPGE current is enhanced with compressive strain rising from 0% to −0.8%, while it is suppressed with tensile strain rising from 0% to +0.8%. The CPGE is 2.6 times enhanced under a 0.8% compressive strain compared with the unstrained one. There-

DOI: 10.1021/acsnano.7b08618
ACS Nano XXXX, XXX, XXX−XXX

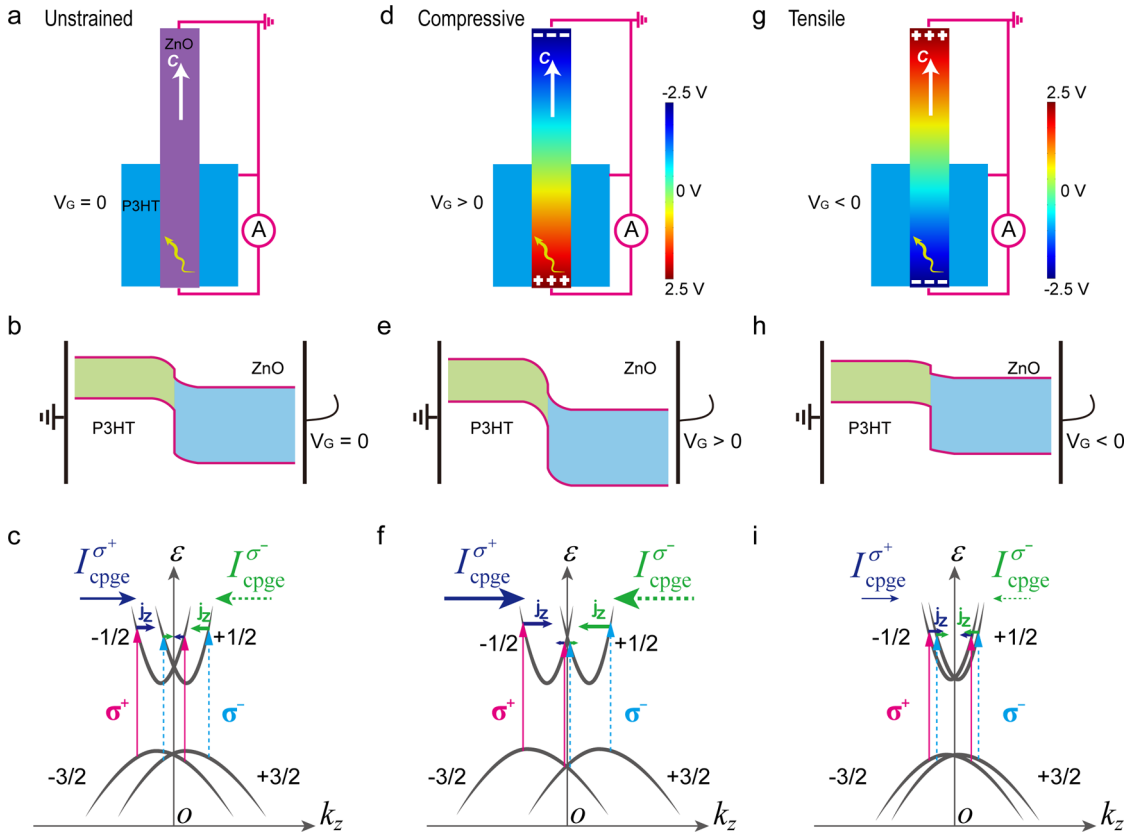

Figure 5. Schematic diagrams of the manipulation of Rashba spin−orbit coupling *via* the piezotronic effect. (a) Schematic diagram of a strain-free sample with a medium CPGE current. (b) Schematic of the energy band of P3HT/ZnO with a gate piezo-potential of 0 V. (c) Schematic diagram for the CPGE current caused by spin splitting of the energy bands when the right (left)-handed circularly polarized light motivates the surface electrons in ZnO NWs to higher energy bands. (d) Schematic diagram of a sample with a compressive strain, illustrating the corresponding piezo-charges and piezo-potential distribution in ZnO. The piezo-potential distribution is numerically simulated by a finite-element analysis method (COMSOL), where the diameter, the length, and the applied pressure are 100 nm, 800 nm, and 60 MPa, respectively. (e) Schematic of energy band of P3HT/ZnO with a positive piezo-potential gate, illustrating an enhanced asymmetry of band structure. (f) Schematic diagram for the enhanced CPGE current caused by an enhanced spin splitting of the energy bands. (g) Schematic diagram of the sample with a tensile strain, illustrating piezo-charges and a piezo-potential distribution opposite of (d). (h) Schematic of the energy band of P3HT/ZnO with a negative piezo-potential gate, illustrating a weakened asymmetry of band structure. (i) Schematic diagram for the decreased CPGE current caused by a weakened spin splitting of the energy bands.

fore, a strong SOC compared with other semiconductor systems is induced in the ZnO/P3HT heterointerface, of which the corresponding CPGE current (~650 nA/W, see Figure 3c) is 8 times larger than that (~80 nA/W) in ZnO thin films,[36] and the current is about 2 orders of magnitude larger than those in InN thin films,[15] GaN/AlGaN hetrojunctions,[49] and n-GaAs quantum wells.[50] Then the amplitudes of CPGE and PV currents (φ = +45°) as a function of strain for an oblique incidence of θ = +45° are counted, as shown in Figure 3d. The amplitudes of CPGE and PV currents decrease almost linearly with strain varying from −0.8% to +0.8%. Possible mechanisms accounting for this will be discussed later.

In order to check if there is a Dresselhaus SOC in the ZnO NW array, we fabricated a device with a ZnO NW array without spin-coating P3HT. In the case of a short circuit of the device, a thin layer of poly(methyl methacrylate) (PMMA) was spin-coated on the as-synthesized ZnO NW array followed by O_2 plasma etching for exposing the heads of the nanowires, as illustrated in Figure 4a. At the very beginning, we believed that the case of only the ZnO nanowire array can induce a detectable CPGE current which can be tuned by strain due to the break in symmetry with the change of the crystal structure itself. The measured photocurrent as a function of phase angle φ for an oblique incidence of θ = +45° under compressive and tensile strains is shown in Figure 4b, from which we can see that there are only LPGE currents and that no obvious CPGE current is found. This is probably because the induced SOC by the change of the crystal structure itself is not strong enough so that we cannot observe a detectable CPGE current at least in this present nanowire array system. As there is no strong spin splitting in the energy band (see Figure 4c) in this device, there is not enough nonequilibrium distribution of photoinduced electrons in momentum space; thus no CPGE current should be observed. This comparison further proves that the n-ZnO/p-P3HT heterointerface indeed induces a strong Rashba SOC. What's more, the piezo-potential induced *via* applying strain in NWs can be effectively used to manipulate the strength of this Rashba SOC. These changing tendencies are in agreement with the result expected from the piezo-potential gate model, to be presented.

Next, we will discuss the piezotronic effect on the Rashba spin−orbit coupling. Since the organic polymer P3HT does not have a piezoelectric effect, our discussions mainly focus on the piezoelectric effect from the ZnO core. ZnO has a noncentral symmetric wurzite structure in which the cations and anions are tetrahedrally coordinated. A strain on the basic unit results in a

DOI: 10.1021/acsnano.7b08618
ACS Nano XXXX, XXX, XXX−XXX

polarization of the cations and anions along the *c*-axis, which is the cause of the piezo-potential inside the crystal. The manipulation of the CPGE current *via* the piezo-potential gate induced by the ZnO NW array under strain can be qualitatively explained through the schematic structure with a numerically calculated piezo-potential distribution, the asymmetry of the band structure at the P3HT/ZnO interface, and a schematic diagram exhibiting the spin splitting of the energy band, as shown in Figure 5. Numerically calculated piezo-potential distributions are simulated by a finite-element analysis method (COMSOL), where the diameter, the length, and the applied pressure are 100 nm, 800 nm, and 60 MPa, respectively. It should be pointed out that the strains displaying in this work (Figure 3 and Figure 4) were calculated actually corresponding to the deformation of the surface of the PET substrate; hence the strains on ZnO NWs should be a bit smaller because of the bigger elasticity modulus of the P3HT/ZnO NW array thin film compared to the PET substrate.

The Ag top electrode contacts both the ZnO nanowires and P3HT (Figure 5a,d,g), which is designed on purpose. Because if one just connects the bottom of the ZnO nanowires and the P3HT, they will detect a strong photovoltaic current due to the inner electric field in the interface of P3HT/ZnO. But one should try to reduce the magnitude of the photovoltaic current in the case of a hidden CPGE current. In other words, although we need to induce an asymmetric interface (P3HT/ZnO), we also have to prevent a photovoltaic effect. Therefore, contacting both ZnO nanowires and P3HT by the Ag top electrode is a good way to share the photovoltaic current; as a result, the photovoltaic current flowing through the current meter will be reduced. At the same time, the CPGE current due to the asymmetric interface (P3HT/ZnO) will flow in the direction parallel to the *c*-axis of ZnO and be collected by the current meter, which is set deliberately to short the circuit of the ZnO NWs. It is the inner spin−orbit coupling due to the asymmetric interface of P3HT/ZnO that induces a spin-related CPGE current of which the direction is just along [0001], and the CPGE electrons will not flow through the p-P3HT.

When the device is measured without applying a strain, the piezo-potential in ZnO is zero, as shown in Figure 5a. The energy band diagram of the ZnO/P3HT interface in this situation can be drawn as in Figure 5b, where the moderate inner built-in electric field results in a structure inversion asymmetry in the normal direction (vertically to the *c*-axis of ZnO NW) of the ZnO/P3HT interface and hence induces a moderate Rashba SOC at the surface of the ZnO NWs. Then, a spin splitting of energy bands due to the moderate Rashba SOC is produced (see Figure 5c). When the circularly polarized light (325 nm) irradiates obliquely on the sample, according to the optical transition selection rule, the spin-polarized electrons will get a nonequilibrium distribution in the k_z direction of the momentum space. As a result, the CPGE currents are detected with opposite signs for left- and right-handed circularly polarized light. When the device is measured under a compressive strain, a piezo-potential distribution along the *c*-axis of ZnO NW is induced with positive piezo-electric charges at the bottom of the as-grown ZnO NW and negative piezo-electric charges at the top of the ZnO NW, as shown in Figure 5d. The piezo-potential close to the bottom of the ZnO NW can be regarded as a positive gate voltage to tune the energy bands of the ZnO/P3HT interface. As shown in Figure 5e, the positive gate piezo-potential lowers the band of the heterointerface at the ZnO side more seriously. However, the gate electric field due to positive gate piezo-potential is applied on the heterointerface and hence enhances the built-in electric field at the heterointerface, which further increases the Rashba SOC at the surface of the ZnO NWs. The enhanced spin splitting of energy bands due to the increased Rashba SOC at the surface of the ZnO NWs results in an increased CPGE current (see Figure 5f and Figure 3d). The Rashba SOC is derived only from the built-in electric field at the interface of ZnO/P3HT. Thus, the Schottky barrier variation of ZnO/Ag contact can affect the PV current; it should not have an effect on Rashba SOC. Actually, the ZnO/Ag forms an ohmic contact.

When the device is measured under a tensile strain, an opposite piezo-potential distribution along the *c*-axis of the ZnO NW is induced with a reversed piezo-electric charge distribution at the ends of the ZnO NW, as shown in Figure 5g. The piezo-potential close to the bottom of the ZnO NW acts as a negative gate voltage and hence offsets the inner built-in electric field at the ZnO/P3HT interface (see Figure 5h), which weakens the structure inversion asymmetry along the normal direction (vertically to the *c*-axis of the ZnO NW) of the interface and further reduces the Rashba SOC at the surface of the ZnO NW. The weakened spin splitting of the energy bands due to the reduced Rashba SOC at the surface (contacting directly with P3HT) of the ZnO NWs results in a decreased CPGE current along the *c*-axis of the ZnO NW (see Figure 5i and Figure 3d). It is the weakened built-in electric field rather than the raising of the band at the ZnO NW bulk that tunes the SIA. When the spin-polarized electrons transport in the ZnO NW, they will also be motivated by the piezo-potential along the nanowire. However, it will be the same for both right-handed and left-handed spin photocurrents, and the influence of the piezo-potential along the NW growth direction on photocurrents should be just a background in PV currents. Meanwhile, the changes of the effective built-in electric field at the ZnO/P3HT interface (see Figure 5e,h) also lead to the enhanced and weakened PV currents for compressive and tensile strains, respectively (see Figure 3d).

There are some arguments on other effects. First, the built-in electric field is distributed within the P3HT/ZnO interface, and the total in-plane built-in electric field is zero. Even if the growth process is controlled precisely, there is still spatial inhomogeneity for a local nanowire array, but it can be neglected if we consider the large area with 2 × 2 mm of the nanowire array (irradiated with a light spot about 1 mm in diameter). Second, the effect of the interaction between nanowires (like enhancement or change in the distribution of the local electric field) is likely to play a part (by possibly breaking the in-plane symmetry) for the CPGE current, but it should be much smaller than the contribution from the piezo-potential. Because a 0.8% strain cannot change too much the deformation of the ZnO nanowires, the change of the distribution of the local electric field should be small. However, the CPGE current under 0.8% compressive strain is 2.6 times enhanced compared with the unstrained one. Such strong modulation of the Rashba SOC is probably due to the large piezo-potential that can be effectively applied on the interface of P3HT/ZnO, but hardly to the small change of the distribution of the local electric field. Third, although the CPGE is usually accompanied by a photovoltaic effect, the photovoltaic effect is just a background for the CPGE, which is a polarization-independent effect (in other words, the photovoltaic effect should not change with the azimuth angle of the quarter-wave plate).

DOI: 10.1021/acsnano.7b08618
ACS Nano XXXX, XXX, XXX−XXX

CONCLUSIONS

In summary, we studied a helicity-dependent photocurrent in a ZnO/P3HT nanowire array structure by illuminating a polarization-tunable light with an oblique angle. We demonstrate a strong Rashba SOC induced by the ZnO/P3HT heterointerface *via* the observation of a CPGE current. With the increase of incident angle, the CPGE current is enhanced under both positive and negative angles. We found that the Rashba SOC at the ZnO/P3HT heterointerface is partially screened by the photovoltaic effect after illumination. On the other hand, we show the study of tuning the Rashba SOC by the inner-crystal piezo-potential (acting as a gate voltage) in ZnO NWs that is generated by applying a strain using the piezotronic effect, instead of applying an external gate voltage. It is worth noting that this mechanism for achieving and modulating the spin photocurrent should not be limited to the ZnO nanowire array structure, our finding can be generalized to other wurtzite piezoelectric nanowires, and the P3HT should also be replaced by other organic layers. The piezo-potential can not only remain steady under a static pressure or strain but also work without the need of extra energy; hence this study shows a promising way of manipulating of Rashba SOC *via* the piezotronic effect on large-scale flexible spintronic devices.

METHODS

Fabrication Processes of the Device. First, thin layers of ITO transparent top electrode (Ar, 100 W, 40 min) and ZnO seed layer (40 sccm Ar, 100 W, 300 nm in thickness) were deposited in turn on a PET substrate (250 μm) by radio frequency (RF) magnetron sputtering (model no. Denton Discovery 635) at room temperature. Then, the coated PET substrate was placed into a mixed nutrient solution (30 mM/L $Zn(NO_3)_2$ and 30 mM/L hexamethylenetetramine (HMTA)) at 90 °C for 40 min for ZnO NW array (patterned with 2 × 2 mm) growth *via* a low-temperature hydrothermal method. In order to increase the growing speed of ZnO nanowires, 2 mL of ammonium hydroxide was added per 60 mL of mixed nutrient solution. After cooling the whole system, the sample was washed by ethanol and distilled water, collected, and dried by high-purity N_2 gas. Next, a thin layer of P3HT (15 mg/mL in chlorobenzene solvent) was spin-coated on the as-synthesized ZnO nanowires at 1000 rpm for 50 s with a spin coater (model no. Smart Coater 100, Best Tools LLC, USA), followed by curing at 100 °C in air for 2 min. Then, the surface of the P3HT-coated ZnO NW array was cleaned by Ar plasma to expose the head of the ZnO NW array. For the compared device in Figure 4, a thin layer of PMMA instead of P3HT was spin-coated on the as-synthesized ZnO NW array followed by O_2 plasma etching for 5 min to expose the heads of the nanowires. The Ag bottom electrode was then deposited on top of the etched ZnO NW array by direct current (dc) magnetron sputtering at room temperature. Two Cu wires were respectively attached on the ITO top electrode and the Ag bottom electrode by silver-epoxy adhesive.

Characterization and Measurement. The detailed microscopic structural and morphological characterizations were carried out with a Hitachi SU8020 field-emission scanning electron microscope. The absorption spectra were obtained with a UV−vis−NIR spectrophotometer (Shimadzu UV3600). The *I*−*V* characteristics of the device were measured and recorded by a customized computer-controlled measurement system with a function generator (model no. DS345, Stanford Research Systems, Inc.) and a low-noise current preamplifier (model no. SR570, Stanford Research Systems, Inc.) in conjunction with a GPIB controller (GPIB-USB-US, NI 488.2). The CPGE measurements were performed at room temperature. The setup for CPGE measurements is illustrated in Supporting Information Figure S6. A He−Cd laser (model no. IK3501R-G, Kimmon Koha Co., Ltd.) with a wavelength of 325 nm was used as the optical excitation source for interband carrier excitation in ZnO. A continuously variable filter was used to control the light intensity. The incident light went through a polarizer and a rotatable quarter-wavelength plate to yield a helicity-modulated incident light. After passing through a chopper (model no. SR540, Stanford Research Systems, Inc.) with a frequency of 220 Hz, the light beam with a diameter of about 1 mm irradiated obliquely on the sample. Then, the induced photocurrents on the sample were amplified by a low-noise current preamplifier (model no. SR570, Stanford Research Systems, Inc.) and then collected by a lock-in amplifier (model no. SR850, Stanford Research Systems, Inc.) with a reference frequency of 220 Hz. Two three-dimensional manual displacement stages were applied to bend the device.

ASSOCIATED CONTENT

Supporting Information

The Supporting Information is available free of charge on the ACS Publications website at DOI: 10.1021/acsnano.7b08618.

Additional information and figures (PDF)

AUTHOR INFORMATION

Corresponding Author

*E-mail: zhong.wang@mse.gatech.edu.

ORCID

Zhong Lin Wang: 0000-0002-5530-0380

Author Contributions

⊥L.Z. and Y.Z. contributed equally to this work.

Notes

The authors declare no competing financial interest.

ACKNOWLEDGMENTS

This research was supported by the "Thousands Talents" Program for Pioneer Researcher and His Innovation Team, China, National Natural Science Foundation of China (Grant Nos. 11704032, 51432005, 5151101243, and 51561145021), the National Key R & D Project from Minister of Science and Technology (2016YFA0202704), the National Program for Support of Top-Notch Young Professionals, and the China Postdoctoral Science Foundation (2016M600067).

REFERENCES

(1) Prinz, G. A. *Magnetoelectronics. Science* **1998**, *282*, 1660−1663.

(2) Wolf, S.; Awschalom, D.; Buhrman, R.; Daughton, J.; Von Molnar, S.; Roukes, M.; Chtchelkanova, A. Y.; Treger, D. Spintronics: A Spin-Based Electronics Vision for the Future. *Science* **2001**, *294*, 1488−1495.

(3) Žutić, I.; Fabian, J.; Das Sarma, S. Spintronics: Fundamentals and Applications. *Rev. Mod. Phys.* **2004**, *76*, 323−410.

(4) Awschalom, D. D.; Flatte, M. E. Challenges for Semiconductor Spintronics. *Nat. Phys.* **2007**, *3*, 153−159.

(5) Yuan, H.; Bahramy, M. S.; Morimoto, K.; Wu, S.; Nomura, K.; Yang, B.-J.; Shimotani, H.; Suzuki, R.; Toh, M.; Kloc, C. Zeeman-Type Spin Splitting Controlled by an Electric Field. *Nat. Phys.* **2013**, *9*, 563.

(6) Kotlyar, R.; Reinecke, T.; Bayer, M.; Forchel, A. Zeeman Spin Splittings in Semiconductor Nanostructures. *Phys. Rev. B: Condens. Matter Mater. Phys.* **2001**, *63*, 085310.

(7) Gammon, D.; Brown, S. W.; Snow, E. S.; Kennedy, T. A.; Katzer, D. S.; Park, D. Nuclear Spectroscopy in Single Quantum Dots: Nanoscopic Raman Scattering and Nuclear Magnetic Resonance. *Science* **1997**, *277*, 85−88.

(8) Ganichev, S.; Prettl, W. Spin Photocurrents in Quantum Wells. *J. Phys.: Condens. Matter* **2003**, *15*, R935.

(9) Ganichev, S. D.; Golub, L. E. Interplay of Rashba/Dresselhaus Spin Splittings Probed by Photogalvanic Spectroscopy−a Review. Phys. *Phys. Status Solidi B* **2014**, *251*, 1801.

(10) Winkler, R. Origin of Spin−Orbit Coupling Effects. In *Spin−Orbit Coupling Effects in Two-Dimensional Electron and Hole Systems*; Springer: Berlin, Heidelberg, 2003; pp 61−68.

DOI: 10.1021/acsnano.7b08618
ACS Nano XXXX, XXX, XXX−XXX

(11) Dresselhaus, G. Spin-Orbit Coupling Effects in Zinc Blende Structures. *Phys. Rev.* **1955**, *100*, 580−586.
(12) Wu, M. W.; Jiang, J. H.; Weng, M. Q. Spin Dynamics in Semiconductors. *Phys. Rep.* **2010**, *493*, 61−236.
(13) Lechner, V.; Golub, L. E.; Olbrich, P.; Stachel, S.; Schuh, D.; Wegscheider, W.; Bel'kov, V. V.; Ganichev, S. D. Tuning of Structure Inversion Asymmetry by the δ-Doping Position in (001)-Grown Gaas Quantum Wells. *Appl. Phys. Lett.* **2009**, *94*, 242109.
(14) Hao, X.-J.; Tu, T.; Cao, G.; Zhou, C.; Li, H.-O.; Guo, G.-C.; Fung, W. Y.; Ji, Z.; Guo, G.-P.; Lu, W. Strong and Tunable Spin−Orbit Coupling of One-Dimensional Holes in Ge/Si Core/Shell Nanowires. *Nano Lett.* **2010**, *10*, 2956−2960.
(15) Yin, C.; Yuan, H.; Wang, X.; Liu, S.; Zhang, S.; Tang, N.; Xu, F.; Chen, Z.; Shimotani, H.; Iwasa, Y.; Chen, Y.; Ge, W.; Shen, B. Tunable Surface Electron Spin Splitting with Electric Double-Layer Transistors Based on InN. *Nano Lett.* **2013**, *13*, 2024−2029.
(16) Liang, D.; Gao, X. P. Strong Tuning of Rashba Spin−Orbit Interaction in Single InAs Nanowires. *Nano Lett.* **2012**, *12*, 3263−3267.
(17) Yin, C.; Shen, B.; Zhang, Q.; Xu, F.; Tang, N.; Cen, L.; Wang, X.; Chen, Y.; Yu, J. Rashba and Dresselhaus Spin-Orbit Coupling in Gan-Based Heterostructures Probed by the Circular Photogalvanic Effect under Uniaxial Strain. *Appl. Phys. Lett.* **2010**, *97*, 181904.
(18) Winkler, R. Rashba Spin Splitting in Two-Dimensional Electron and Hole Systems. *Phys. Rev. B: Condens. Matter Mater. Phys.* **2000**, *62*, 4245−4248.
(19) Lipparini, E.; Barranco, M.; Malet, F.; Pi, M.; Serra, L. Spin-Orbit Effects in GaAs Quantum Wells: Interplay between Rashba, Dresselhaus, and Zeeman Interactions. *Phys. Rev. B: Condens. Matter Mater. Phys.* **2006**, *74*, 115303.
(20) Ganichev, S. D.; Bel'kov, V. V.; Golub, L. E.; Ivchenko, E. L.; Schneider, P.; Giglberger, S.; Eroms, J.; De Boeck, J.; Borghs, G.; Wegscheider, W.; Weiss, D.; Prettl, W. Experimental Separation of Rashba and Dresselhaus Spin Splittings in Semiconductor Quantum Wells. *Phys. Rev. Lett.* **2004**, *92*, 256601.
(21) Zhu, L.; Liu, Y.; Jiang, C.; Yu, J.; Gao, H.; Ma, H.; Qin, X.; Li, Y.; Wu, Q.; Chen, Y. Spin Depolarization under Low Electric Fields at Low Temperatures in Undoped InGaAs/AlGaAs Multiple Quantum Well. *Appl. Phys. Lett.* **2014**, *105*, 152103.
(22) LaShell, S.; McDougall, B. A.; Jensen, E. Spin Splitting of an Au(111) Surface State Band Observed with Angle Resolved Photoelectron Spectroscopy. *Phys. Rev. Lett.* **1996**, *77*, 3419−3422.
(23) Varykhalov, A.; Marchenko, D.; Scholz, M. R.; Rienks, E. D. L.; Kim, T. K.; Bihlmayer, G.; Sánchez-Barriga, J.; Rader, O. Ir(111) Surface State with Giant Rashba Splitting Persists under Graphene in Air. *Phys. Rev. Lett.* **2012**, *108*, 066804.
(24) Ast, C. R.; Henk, J.; Ernst, A.; Moreschini, L.; Falub, M. C.; Pacilé, D.; Bruno, P.; Kern, K.; Grioni, M. Giant Spin Splitting through Surface Alloying. *Phys. Rev. Lett.* **2007**, *98*, 186807.
(25) Leppert, L.; Reyes-Lillo, S. E.; Neaton, J. B. Electric Field- and Strain-Induced Rashba Effect in Hybrid Halide Perovskites. *J. Phys. Chem. Lett.* **2016**, *7*, 3683−3689.
(26) Etienne, T.; Mosconi, E.; De Angelis, F. Dynamical Origin of the Rashba Effect in Organohalide Lead Perovskites: A Key to Suppressed Carrier Recombination in Perovskite Solar Cells? *J. Phys. Chem. Lett.* **2016**, *7*, 1638−1645.
(27) Li, J.; Haney, P. M. Circular Photogalvanic Effect in Organometal Halide Perovskite $CH_3NH_3PbI_3$. *Appl. Phys. Lett.* **2016**, *109*, 193903.
(28) King, P. D. C.; Hatch, R. C.; Bianchi, M.; Ovsyannikov, R.; Lupulescu, C.; Landolt, G.; Slomski, B.; Dil, J. H.; Guan, D.; Mi, J. L.; Rienks, E. D. L.; Fink, J.; Lindblad, A.; Svensson, S.; Bao, S.; Balakrishnan, G.; Iversen, B. B.; Osterwalder, J.; Eberhardt, W.; Baumberger, F.; Hofmann, P. Large Tunable Rashba Spin Splitting of a Two-Dimensional Electron Gas in Bi_2Se_3. *Phys. Rev. Lett.* **2011**, *107*, 096802.
(29) Yuan, H.; Wang, X.; Lian, B.; Zhang, H.; Fang, X.; Shen, B.; Xu, G.; Xu, Y.; Zhang, S.-C.; Hwang, H. Y. Generation and Electric Control of Spin-Valley-Coupled Circular Photogalvanic Current in WSe_2. *Nat. Nanotechnol.* **2014**, *9*, 851−857.
(30) Ishizaka, K.; Bahramy, M. S.; Murakawa, H.; Sakano, M.; Shimojima, T.; Sonobe, T.; Koizumi, K.; Shin, S.; Miyahara, H.; Kimura, A.; Miyamoto, K.; Okuda, T.; Namatame, H.; Taniguchi, M.; Arita, R.; Nagaosa, N.; Kobayashi, K.; Murakami, Y.; Kumai, R.; Kaneko, Y.; Onose, Y.; Tokura, Y. Giant Rashba-Type Spin Splitting in Bulk BiTeI. *Nat. Mater.* **2011**, *10*, 521−526.
(31) Singh, S.; Romero, A. H. Giant Tunable Rashba Spin Splitting in a Two-Dimensional BiSb Monolayer and in BiSb/AlN Heterostructures. *Phys. Rev. B: Condens. Matter Mater. Phys.* **2017**, *95*, 165444.
(32) Look, D. C. Recent Advances in ZnO Materials and Devices. *Mater. Sci. Eng., B* **2001**, *80*, 383−387.
(33) Anderson, J.; Chris, G. V. d. W. Fundamentals of Zinc Oxide as a Semiconductor. *Rep. Prog. Phys.* **2009**, *72*, 126501.
(34) Wang, Z. L. Piezopotential Gated Nanowire Devices: Piezotronics and Piezo-Phototronics. *Nano Today* **2010**, *5*, 540−552.
(35) Ghosh, S.; Sih, V.; Lau, W. H.; Awschalom, D. D.; Bae, S. Y.; Wang, S.; Vaidya, S.; Chapline, G. Room-Temperature Spin Coherence in ZnO. *Appl. Phys. Lett.* **2005**, *86*, 232507.
(36) Zhang, Q.; Wang, X.; Yin, C.; Xu, F.; Tang, N.; Shen, B.; Chen, Y.; Chang, K.; Ge, W.; Ishitani, Y. Strong Circular Photogalvanic Effect in ZnO Epitaxial Films. *Appl. Phys. Lett.* **2010**, *97*, 041907.
(37) Prestgard, M. C.; Siegel, G.; Roundy, R.; Raikh, M.; Tiwari, A. Temperature Dependence of the Spin Relaxation in Highly Degenerate ZnO Thin Films. *J. Appl. Phys.* **2015**, *117*, 083905.
(38) Liu, W. K.; Whitaker, K. M.; Smith, A. L.; Kittilstved, K. R.; Robinson, B. H.; Gamelin, D. R. Room-Temperature Electron Spin Dynamics in Free-Standing ZnO Quantum Dots. *Phys. Rev. Lett.* **2007**, *98*, 186804.
(39) Janssen, N.; Hanke, T.; Sotier, F.; Thomay, T.; Bratschitsch, R.; Whitaker, K. M.; Gamelin, D. R. Ultrafast Spin Dynamics in Colloidal ZnO Quantum Dots. *Nano Lett.* **2008**, *8*, 1991−1994.
(40) Liu, W.; Lee, M.; Ding, L.; Liu, J.; Wang, Z. L. Piezopotential Gated Nanowire−Nanotube Hybrid Field-Effect Transistor. *Nano Lett.* **2010**, *10*, 3084−3089.
(41) Wu, W.; Wen, X.; Wang, Z. L. Taxel-Addressable Matrix of Vertical-Nanowire Piezotronic Transistors for Active and Adaptive Tactile Imaging. *Science* **2013**, *340*, 952.
(42) Wu, W.; Pan, C.; Zhang, Y.; Wen, X.; Wang, Z. L. Piezotronics and Piezo-Phototronics - from Single Nanodevices to Array of Devices and Then to Integrated Functional System. *Nano Today* **2013**, *8*, 619−642.
(43) Wu, W.; Wang, L.; Li, Y.; Zhang, F.; Lin, L.; Niu, S.; Chenet, D.; Zhang, X.; Hao, Y.; Heinz, T. F.; Hone, J.; Wang, Z. L. Piezoelectricity of Single-Atomic-Layer MoS2 for Energy Conversion and Piezotronics. *Nature* **2014**, *514*, 470−474.
(44) Jiang, C.; Shalygin, V.; Panevin, V. Y.; Danilov, S.; Glazov, M.; Yakimova, R.; Lara-Avila, S.; Kubatkin, S.; Ganichev, S. Helicity-Dependent Photocurrents in Graphene Layers Excited by Midinfrared Radiation of a CO_2 Laser. *Phys. Rev. B: Condens. Matter Mater. Phys.* **2011**, *84*, 125429.
(45) Yang, C. L.; He, H. T.; Ding, L.; Cui, L. J.; Zeng, Y. P.; Wang, J. N.; Ge, W. K. Spectral Dependence of Spin Photocurrent and Current-Induced Spin Polarization in an InGaAs/InAlAs Two-Dimensional Electron Gas. *Phys. Rev. Lett.* **2006**, *96*, 186605.
(46) Yu, J.; Chen, Y.; Liu, Y.; Jiang, C.; Ma, H.; Zhu, L. Spectra of Rashba-and Dresselhaus-Type Circular Photogalvanic Effect at Inter-Band Excitation in GaAs/AlGaAs Quantum Wells and Their Behaviors under External Strain. *Appl. Phys. Lett.* **2012**, *100*, 152110.
(47) Zhou, W. Z.; Lin, T.; Shang, L. Y.; Sun, L.; Gao, K. H.; Zhou, Y. M.; Yu, G.; Tang, N.; Han, K.; Shen, B.; Guo, S. L.; Gui, Y. S.; Chu, J. H. Influence of the Illumination on Weak Antilocalization in an $Al_xGa_{1-x}N$/GaN Heterostructure with Strong Spin-Orbit Coupling. *Appl. Phys. Lett.* **2008**, *93*, 262104.
(48) Tang, N.; Shen, B.; He, X.-W.; Han, K.; Yang, Z.-J.; Qin, Z.-X.; Zhang, G.-Y.; Lin, T.; Zhu, B.; Zhou, W.-Z.; Shang, L.-Y.; Chu, J.-H. Influence of the Illumination on the Beating Patterns in the Oscillatory

DOI: 10.1021/acsnano.7b08618
ACS Nano XXXX, XXX, XXX−XXX

Magnetoresistance in $Al_xGa_{1-x}N$/GaN Heterostructures. *Phys. Rev. B: Condens. Matter Mater. Phys.* **2007**, *76*, 155303.
(49) Wittmann, B.; Golub, L.; Danilov, S.; Karch, J.; Reitmaier, C.; Kvon, Z.; Vinh, N.; van der Meer, A.; Murdin, B.; Ganichev, S. Resonant Circular Photogalvanic Effect in GaN/AlGaN Heterojunctions. *Phys. Rev. B: Condens. Matter Mater. Phys.* **2008**, *78*, 205435.
(50) Ganichev, S.; Bel'kov, V.; Schneider, P.; Ivchenko, E.; Tarasenko, S.; Wegscheider, W.; Weiss, D.; Schuh, D.; Beregulin, E.; Prettl, W. Resonant Inversion of the Circular Photogalvanic Effect in N-Doped Quantum Wells. *Phys. Rev. B: Condens. Matter Mater. Phys.* **2003**, *68*, 035319.

DOI: 10.1021/acsnano.7b08618
ACS Nano XXXX, XXX, XXX−XXX